On the Attenuation of Ultrasound by Pure Black Tattoo Ink

Craig S. Carlson, *Member, SAIEE*, *Member, IEEE*, Aurélie Deroubaix, Clement Penny, and Michiel Postema, *Senior Member, IEEE*

***Abstract*—Black tattoo ink comprises hydrophobic carbon black nanoparticles. We hypothesized that black tattoo ink demonstrates transient dynamic activity in an ultrasound field. Brightness-mode sonography was performed on cylindrical receptacles of different bore diameters, filled with black tattoo ink, water, saline, or air, using pulsed ultrasound with center frequencies of 13 MHz and 5 MHz.**

The scattering from black ink itself lasted less than ten minutes. At 13-MHz sonication, a transient drop in sound speed was observed, as well as a transient lessening of scattering from distal phantom tissue. The linear acoustic attenuation coefficient of pure black ink was measured to be 0.15 ± 0.01 dB cm^{-1} MHz^{-1}, equal to whole blood.

Low-intensity ultrasonic tattoo removal would be of interest as an alternative to techniques that damage surrounding tissue.

***Index Terms*—Carbon black, C65 acoustics, high-frequency sonication, diagnostic ultrasound, particle detection, tattoo detection, hydrophobic nanoparticles.**

I. Introduction

TATTOOS have been under investigation for their role in society [1, 2], in physical health [3–6], and even in mental health [7, 8]. Ultrasonic imaging has been used to monitor dermatological tattoo complications [9, 10]. In addition to laser ablation [11], ultrasound has also been experimentally applied for tattoo removal [12, 13]. The high-intensity focussed ultrasound used for this purpose ablates the tissue in or near the transducer focus, irrespective of the presence of ink. To date, no studies have investigated the acoustic properties of tattoo ink particles themselves and their response to an incident low-amplitude sound field.

The most common tattoo color is black [14, 15]. As the vast majority of tattoo-related medical complaints result from black tattoo ink [15, 16], this type of ink is the primary focus in tattoo modification and removal. Black tattoo ink comprises carbon black nanoparticles [17, 18]. As carbon black nanoparticles demonstrate transient dynamic activity in an ultrasound field [19], we hypothesize that black tattoo ink exhibits similar behavior. The purpose of this study is to investigate transient and steady-state behavior of black tattoo ink under sonication.

C.S.C. and M.P. are with the School of Electrical and Information Engineering, University of the Witwatersrand, Johannesburg, 1 Jan Smuts Laan, Braamfontein 2050, South Africa (e-mail: michiel.postema@wits.ac.za). A.D. and C.P. are with the School of Clinical Medicine, University of the Witwatersrand, Johannesburg, 7 York Road, 2193 Parktown, South Africa. M.P. is also with BioMediTech, Faculty of Medicine and Health Technology, Tampere University, Korkeakoulunkatu 3, 33720 Tampere, Finland.

Manuscript received April 21, 2020; revised September 27, 2020; accepted November 4, 2020.

Although an early study on the interaction of ultrasound and carbon black was applied to the identification of components for smart battery recycling [20], our primary long-term purpose with the present study is to deposit acoustic energy into particles suitable for superficial human injection, thereby directly heating the particles and indirectly the surrounding tissue. This might facilitate sonic tattoo removal at low, nondestructive acoustic intensities.

Numerous studies have been dedicated to the experimental determination of the sound-absorbing properties of biological tissue [21–25], tissue-mimicking phantoms [26, 27], salty water [28, 29], and combinations thereof [30]. Although their structures may appear solid, from a physics point of view, most tissues studied in medical ultrasonography are considered fluids [31].

Sound absorption in fluids can be mainly attributed to viscous and thermal damping. The viscous damping corresponds to the friction associated with the relative motion of the particles. The viscous damping coefficient in fluids is proportional to the squared transmission frequency. Thermal damping is the mechanism whereby a fraction of the energy carried by the propagating wave is converted into heat by thermoelasticity. In most liquids and solids, the thermal damping coefficient can be neglected, but in gases it accounts for roughly a third of the total damping [31]. Consequently, bulk fluid absorbs sound better if there is gas presence. If the gas presence is transient, so must the absorption. Hydrophobic particles in suspension have a gaseous surrounding layer, referred to as a void [32]. This void is compressible. Just like all other compressible

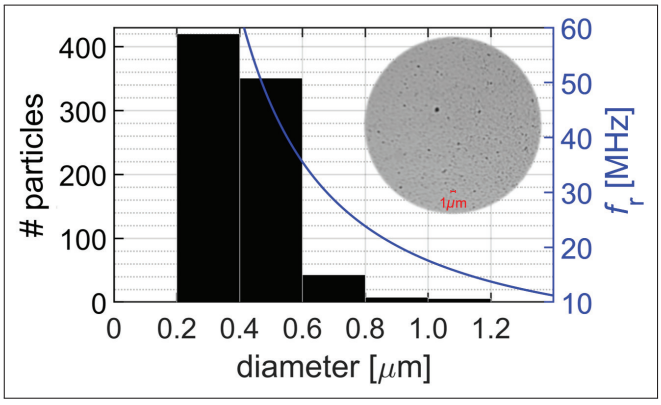

Fig. 1. Size distribution of Zuper Black pigment dispersion (histogram) and particle resonance frequency as a function of the diameter (curve), with an inlay of a bright-field microscopy image of a 0.01% dilution of Zuper Black at 63× magnification.

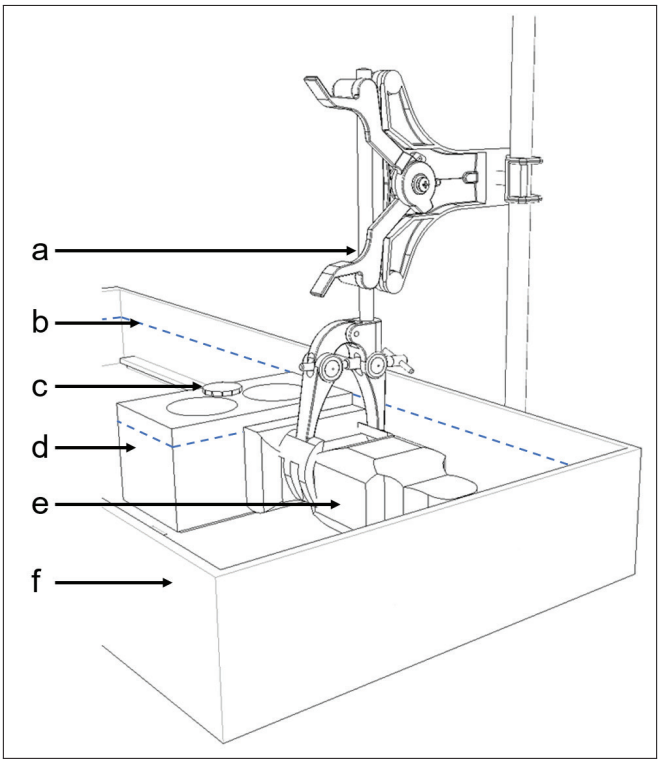

Fig. 2. Line drawing of the experimental setup, consisting of a burette clamp and stand (a), water, whose level is indicated by a blue dashed line (b), a £1 coin for scale (c), a tissue-mimicking phantom receptacle (d), an ultrasound probe (e), and a Perspex container (f).

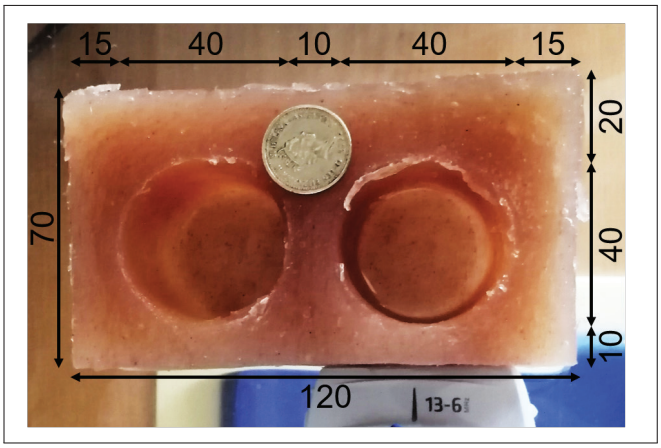

Fig. 3. Top view of the tissue-mimicking phantom receptacle with two cylindrical wells. Dimensions are in mm.

entities, hydrophobic particles in suspension can oscillate, move, attract, and repel each other under the influence of sound, owing to so-called Bjerknes forces [33].

Hydrophobic carbon black nanoparticles are only transiently acoustically active [34]. Some of these particles have been observed to lose their surrounding voids whilst oscillating. Once dehydrophobised, they appeared to remain inactive in an ultrasound field [19]. Consequently, we speculate, that the state of hydrophobicity must influence the thermal damping of ultrasound propagating through the fluid. The voids, once released, become free gas microbubbles. These must dissolve within milliseconds [31]. The presence of freely oscillating microbubbles must influence the speed of sound in the medium [33].

The ultrasonic transmission frequencies used in [19, 34] were 45 kHz and 1 MHz. These frequencies were much lower than the resonance frequencies of the particles under sonication. To exploit Bjerknes forces for actual physical manipulation of nanoparticles, one would need to sonicate at a frequency much closer to the resonance frequencies of the particles [31].

The resonance frequency of a hydrophobic particle can be estimated from [35], where the optically observed radius of a particle in suspension, which includes the void, is taken for the outer radius, and the dry particle radius is taken for the inner radius. It is noted that the derivation of the oscillating and translating dynamics of a spherically symmetric hydrophobic particle is identical to that of an antibubble [36]. It is also noted that the largest particles in a population contribute most to the acoustic response of that population [33]. In a preliminary study, the acoustic conditions for tattoo removal were modeled assuming ink particle sizes greater than 50 μm [37]. This assumption is, for some inks, a factor of 1000 off, as black ink particles may be as small as 40 nm in diameter [17, 38]. Using atomic force microscopy, the diameters of black ink particles were measured to have a mode of 0.24 μm [38]. The largest black ink particle had a diameter of 0.97 μm [38].

To determine which ultrasonic frequency to use in our experiments, we needed to measure the size distribution of the black ink particles in solution and to compute the corresponding resonance frequencies.

In this study, ultrasound images from a diagnostic scanner were recorded from black tattoo ink contained in various receptacles, with a focus on the variation of backscattering over time from the ink and from distal scatterers.

II. Materials and Methods

Zuper Black pigment dispersion (INTENZE Products, Inc., Rochelle Park, NJ, USA) was used for black ink. Undiluted black ink was measured to have a density of 1313 kg m^{-3}.

For size distribution estimation, bright-field microscopy images were captured of a 0.01% dilution of Zuper Black using the bright-field component of a ZEISS LSM 780 confocal laser scanning microscope with an alpha Plan-Apochromat 63×/1.40 NA Oil CorrM27 objective lens (Carl Zeiss AG, Oberkochen, Germany) [39].

Figure 1 shows the size distribution histogram and a graph of the particle resonance frequency as a function of its diameter. The mode of the diameters measured was 0.29 μm and the largest diameter was 1.14 μm. Dividing the dry particle mode from [38] by the mode measured from our wet ink particles, and dividing the largest particle diameter from [38] by our largest wet particle diameter yielded $\frac{0.24\,\mu\text{m}}{0.29\,\mu\text{m}} \approx \frac{0.97\,\mu\text{m}}{1.14\,\mu\text{m}} \approx 0.8$. Thus, the resonance frequencies were computed from [35, eq. 1], approximating the inner-to-outer diameter ratio by 0.8. Our largest particle had a resonance frequency of 15 MHz. All other ink particles had greater resonance frequencies than 15 MHz. To be certain that all particles oscillated in anti-phase

with respect to the incident sound field [31], we chose operating frequencies slightly less, at 13 MHz, and substantially less, at 5 MHz.

Our ultrasonic experiments were carried out in a Perspex container of 580×235×65 $(\text{mm})^3$ internal dimensions, which was filled with degassed water. A line drawing of the experimental setup is shown in Figure 2. The setup had been designed for optically observing microscopic biomaterials under sonication [40, 41].

Either an HFL38 13–6 MHz linear probe or a C60 5–2 MHz curvilinear probe of a SonoSite® M-Turbo® sonography device (FUJIFILM SonoSite, Inc., Bothell, WA, USA) was clamped in the length direction of the container. The sonography device was operating in either intima-media thickness (IMT) or nerve (Nrv) brightness mode. IMT was the default operating mode for the 13–6 MHz probe; Nrv was the default operating mode for the 5–2 MHz probe. The ultrasound penetration depths of the 13–6 MHz probe and the 5–2 MHz probe were set to 6.0 cm and 6.6 cm, respectively.

The sonography device converted two-way travel times to one-way radial distances assuming c_t=1540 $\text{m}\,\text{s}^{-1}$ for the speed of sound in tissue. It compensated for tissue attenuation by amplifying the backscattered signal by 0.3 $\text{dB}\,\text{cm}^{-1}\text{MHz}^{-1}$ by default [22, 42]. In both operating modes, the mechanical and thermal indices had fixed values of 0.6 and 0.1, respectively. Automatic image adjustments had been switched off.

Two tissue-mimicking phantom receptacles with empty cylindrical wells were manufactured according to the method in [43]. A picture of one of the phantom receptacles and its dimensions is shown in Figure 3.

The phantom material was measured to have a density of 1025 $\text{kg}\,\text{m}^{-3}$, a speed of sound of approximately 1500 $\text{m}\,\text{s}^{-1}$, and a linear attenuation coefficient of 0.35 $\text{dB}\,\text{cm}^{-1}\,\text{MHz}^{-1}$. A phantom receptacle was placed in the container such that one of its sides touched the probe surface.

Other receptacles used in this study were CUPROPHAN® RC55 cellulose capillaries (Membrana GmbH, Wuppertal, Germany) with a 200-μm bore diameter and an 8-μm wall thickness, and RS PRO silicone transparent Silicone Tubing (RS Components (SA), Midrand, South Africa) with a 0.50-mm bore diameter.

Whilst the phantom receptacles were at a fixed position in the container, our most modest receptacles were manually held between 0.6 cm and 1.3 cm in front of the 13–6 MHz probe. For these receptacles, the ultrasound penetration depth was adjusted to 1.8 cm.

The phantom receptacle wells were filled with pure (undiluted) ink using a syringe. The silicone tubes were filled with a 25% dilution using a syringe and the capillaries were filled with a 25% dilution using capillary action. These receptacles were used for calibration and illustration purposes. As the ink had been diluted, these experiments were not used for quantification. For control experiments, receptacles filled with degassed Braamfontein tap water, Reitzer's Distilled Water (Reitzer Pharmaceuticals, Kempton Park, South Africa), SABAX Pour Saline 0,9% (Adcock Ingram Critical Care (Pty) Ltd, Midrand, South Africa), phantom tissue, and air were used.

Sonication continued for ten minutes after each filling, during which images were recorded.

The experiments with the phantom receptacles took place over two consecutive days, the experiments with the other receptacles took place on two separate days. A total of 553 brightness-mode still-frames were recorded using the ultrasound scanner internal storage.

Image processing was done using MATLAB® (The MathWorks, Inc., Natick, MA, USA). In all images recorded, the axial backscattering profiles were extracted on an 8-bit gray scale, after which the absolute peak scatter amplitudes, corresponding to the proximal and distal receptacle interfaces, were measured. In selected images, the mean of the axial scattering from the far field, distal to the last interface, was measured.

The linear acoustic attenuation coefficients of the media under investigation were computed, correcting for tissue attenuation compensation of the device [42] and taking into account the geometric spreading of a point scatterer and a dual interface system with opposing reflection coefficients [44]:

$$e^{2f_\text{c}[\alpha_n(r_2-r_1)-\alpha_\text{t}(r_2'-r_1')]}=\frac{p_1}{p_2}\frac{r_1}{r_2}(1+R_n)(1-R_n), \quad (1)$$

where f_c is the center frequency of the ultrasound pulse, p_1 is the proximal peak, p_2 is the distal peak, r_1 is the axial distance to the proximal interface, r_1' is the perceived distance to the proximal interface, r_2 is the axial distance to the distal interface, r_2' is the perceived distance to the distal interface, α_n is the acoustic attenuation coefficient of medium n, α_t is the average attenuation coefficient in soft tissue [22], and R_n is the pressure reflection coefficient at the proximal interface, given by

$$R_n=\frac{\rho_n c_n-\rho_\phi c_\phi}{\rho_n c_n+\rho_\phi c_\phi}, \quad (2)$$

in which c_n is the speed of sound in medium n, c_ϕ is the speed of sound in the phantom material, ρ_n is the density of medium n, and ρ_ϕ is the density of the phantom material. The units of the attenuation coefficients computed were converted from [$\text{Np}\,\text{m}^{-1}\,\text{MHz}^{-1}$] to [$\text{dB}\,\text{cm}^{-1}\,\text{MHz}^{-1}$] by multiplication by a factor $2000\log_{10}e$.

A change in the speed of sound in the well medium must result in a change in the perceived distance to the distal interface. The time-dependent speed of sound of medium n was computed using

$$c_n(t)=\frac{r_2-r_1}{r_2'(t)-r_1'}\,c_\text{t}. \quad (3)$$

The speed of sound directly measured from (3) was evaluated, knowing that, at a given distance r_1, for a probe with source function $A\,r_0$, the ratio of scattered amplitudes from the proximal interface

$$\frac{p_{1,n+1}(t)}{p_{1,n}}=\frac{\frac{Ar_0}{r_1}e^{2f_\text{c}(\alpha_\text{t}r_1'-\alpha_\phi r_1)}\,|R_{n+1}(t)|}{\frac{Ar_0}{r_1}e^{2f_\text{c}(\alpha_\text{t}r_1'-\alpha_\phi r_1)}\,|R_n|}=\left|\frac{R_{n+1}(t)}{R_n}\right| \quad (4)$$

must equal the ratio of reflection coefficients for different well media, yielding

$$\frac{p_{1,n+1}(t)}{p_{1,n}}=\left|\frac{\rho_{n+1}c_{n+1}(t)-\rho_\phi c_\phi}{\rho_n c_n-\rho_\phi c_\phi}\right|. \quad (5)$$

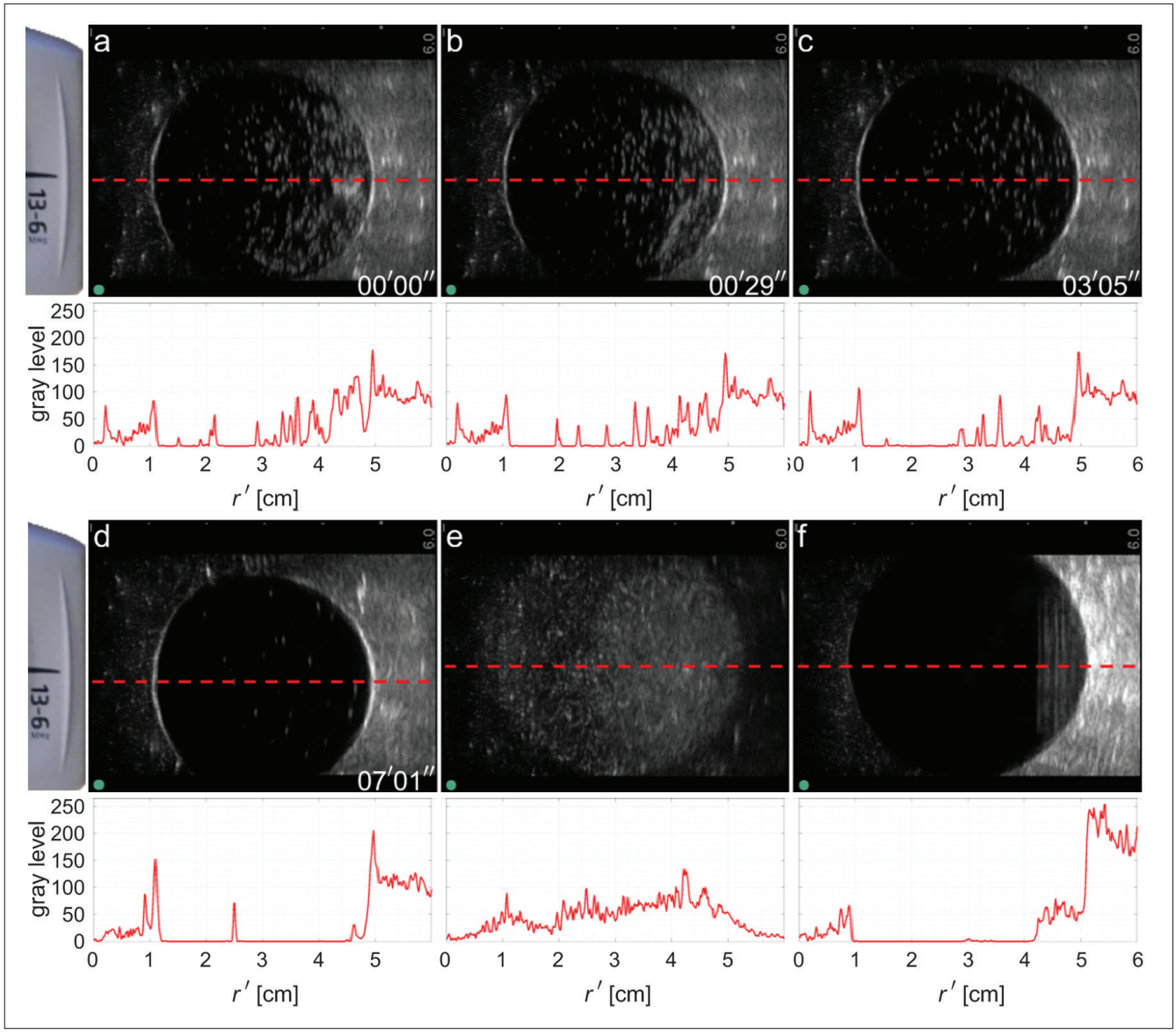

Fig. 4. Brightness-mode scans at a 13-MHz ultrasound frequency of a phantom receptacle well filled with black ink (a–d), phantom material (e), and distilled water (f); and corresponding axial backscattering profiles [8-bit gray scale] as a function of perceived distance [cm]. Time stamps are relative to (a). The green dot corresponds to the right-hand side of the probe.

The influence of nucleation on the attenuation coefficient was estimated by substituting the mean gray level distal of the distal interface for p_2 in (1) and multiplying the right-hand side by $(1+R_n)(1-R_n)$ once more, adding an extra transmission interface. Note that r_2 is not changed, as the size of the well has not changed.

To confirm the receptacle parameters, distilled water was used in control experiments in the wells.

III. Results and Discussion

Figure 4 shows 13-MHz brightness-mode scans of a phantom receptacle well with a 40-mm bore diameter and their respective axial profiles. The bright spots inside the circular areas in frames (a–d) indicate scatterers inside the black ink. The number of scatterers decreased over time, but a few are still visible in frame (d).

The axial backscatter of the ink-filled well shows first peaks at a 1-cm axial distance with 8-bit gray levels rising from 84 (a) to 152 (d). These peaks correspond to the proximal phantom–well interface. The second peaks, at a 5-cm axial distance, correspond to the distal phantom–well interface. These second-peak values rose from 199 to 215 during the $7'01''$ image sequence. Although not visible with the naked eye, the perceived distance between the peaks is 0.16 mm less between frames (c) and (d), indicating a change in the speed of sound. From (3), it followed that the speed of sound of ink was $1621\,\mathrm{m\,s^{-1}}$ in (a) and $1627\,\mathrm{m\,s^{-1}}$ in (d).

The axial backscatter of the water-filled well had a proximal peak gray levels of 67 and a distal level of 244. Substituting the values obtained from (3) into the right-hand side of (4) resulted in a reflection coefficient ratio between ink (d) and water (f) of -2.25. The ratio of proximal peaks in (d) and (e) was

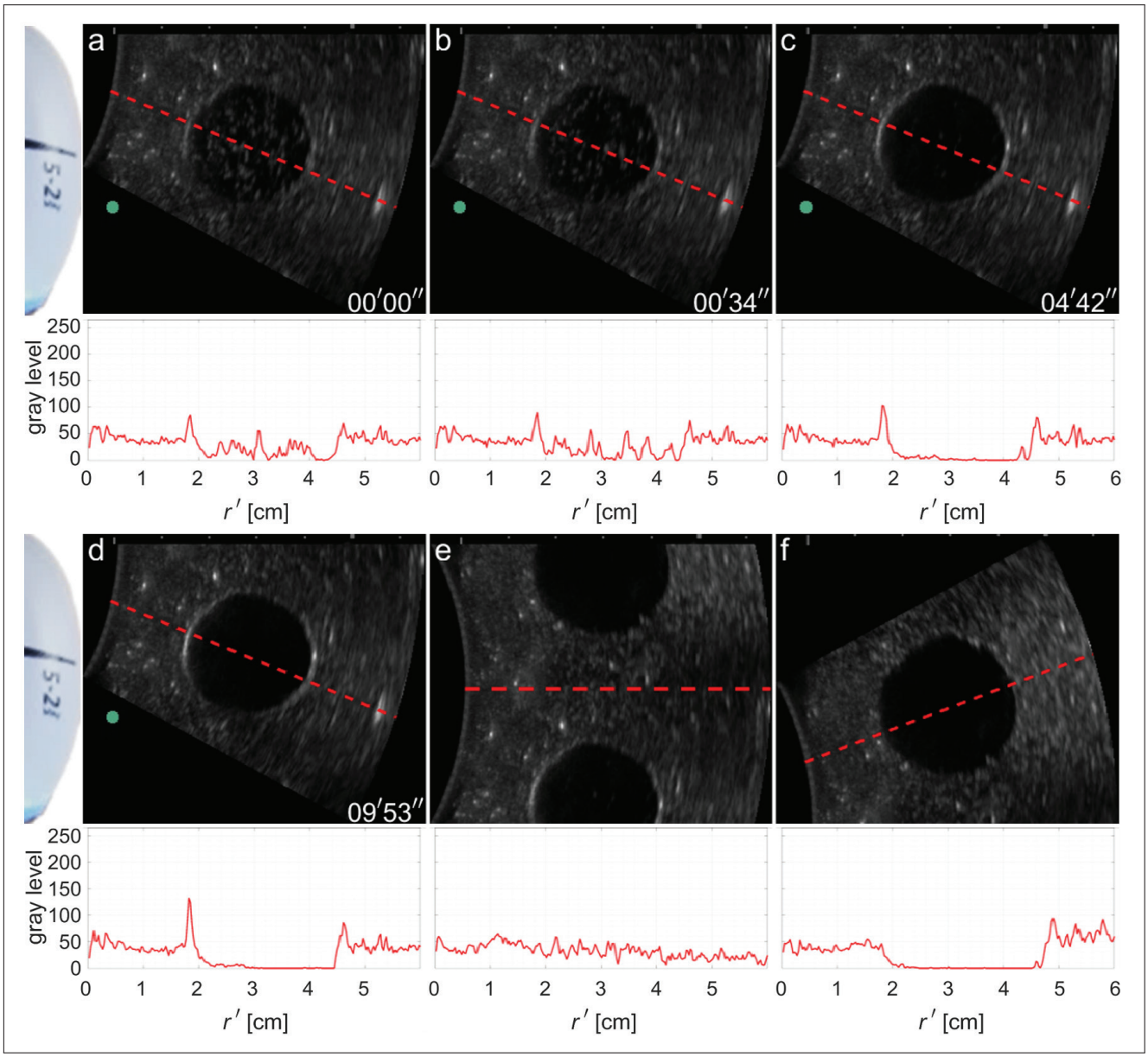

Fig. 5. Brightness-mode scans at a 5-MHz ultrasound frequency of a phantom receptacle well filled with black ink (a–d), phantom material (e), and saline (f); and corresponding axial backscattering profiles [8-bit gray scale] as a function of perceived distance [cm]. Time stamps are relative to (a). The green dot corresponds to the right-hand side of the probe.

2.27. Thus, compared to the level from ink, this low proximal amplitude of distilled water can be attributed to the difference in reflection coefficients. Although the density of nucleating ink could not be measured directly, it could be computed from (5), using (4) as pressure-ratio input. The density of nucleating ink was computed to be around $1200\,\mathrm{kg\,m^{-3}}$ in frame (a). Knowing the steady-state density of black ink, this result means that gas comprises 9% of the volume fraction of nucleating ink. This indicates that the cavitation activity is very dynamic.

The device compensation for tissue attenuation created a 16-dB amplification between the two interfaces. Therefore, the scattering from nucleation is actually not just taking place in the distal part of the well cross section, but over the whole cross section. This is supported by the gradient of the gray level as a function of r' inside the well. The higher distal peak levels in frames (a–d) and (f) are also explained from the lack of attenuation of both media compared to the tissue attenuation compensation. The ink distal peak was portrayed 20 dB higher, the distilled water peak 32 dB. The reflection coefficient played only a minor role in the distal peak amplitude: $|R_n|(1+R_n)(1-R_n)$ is $+2$ dB for ink and -1 dB for distilled water.

Another indicator of cavitation dynamics is the mean gray level distal to the distal interface. In frames (a–d), the mean distal gray level gradually rose from 96 in (a) to 111 in (d). The mean distal gray level of distilled water (f) was 201. Here, the transmission coefficient played a minor role in the scattered amplitude of a phantom speckle: $(1+R_n)^2(1-R_n)^2$ is -2 dB for ink and $+1$ dB for distilled water. These are, however,

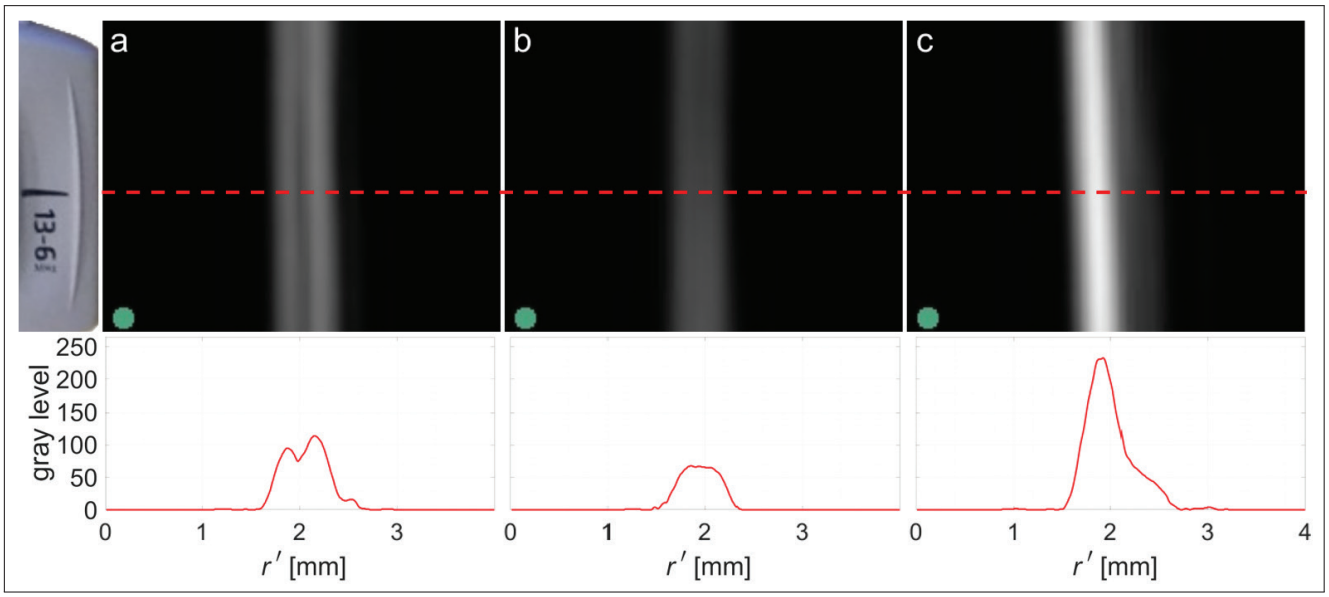

Fig. 6. Brightness-mode scans of capillaries filled with black ink (a), degassed water (b), and air (c); and their respective axial backscattering profiles on an 8-bit gray scale. The green dot corresponds to the right-hand side of the probe.

negligible compared to the device amplification. Therefore, both media have an increased distal gray level, depending on their own attenuation coefficient. As the phantom material itself had an attenuation coefficient slightly higher than that used for tissue compensation, the gray level in (e) gradually declined with distance r according to $e^{-2(\alpha_\phi-\alpha_t)f_c r}$, in addition to the geometric decline according to r^{-1}. Cavitation activity was also reflected by the attenuation coefficient itself. The attenuation coefficient had increased to approximately $0.2\,\mathrm{dB\,cm^{-1}\,MHz^{-1}}$ in frames (a–d). Its steady state-value was $0.15\pm0.01\,\mathrm{dB\,cm^{-1}\,MHz^{-1}}$, measured in a subsequent image sequence, $13'31''$ later (not shown).

The attenuation coefficient of the carbon black pigment dispersion in steady-state, $0.15\,\mathrm{dB\,cm^{-1}\,MHz^{-1}}$, corresponds to the attenuation coefficient of whole blood [22] and is just $0.02\,\mathrm{dB\,cm^{-1}\,MHz^{-1}}$ less than the attenuation coefficient of testes [21]. The attenuation coefficient found for distilled water was $0.00\pm0.01\,\mathrm{dB\,cm^{-1}\,MHz^{-1}}$, which corresponds to the literature value of $0.002\,\mathrm{dB\,cm^{-1}\,MHz^{-1}}$ [30]. Our attenuation coefficient for saline, 0.02 ± 0.02, corresponds to the literature value $0.01\,\mathrm{dB\,cm^{-1}\,MHz^{-1}}$ [30]. The steady-state speeds of sound were measured to be $1639\,\mathrm{m\,s^{-1}}$ of ink; of saline $1568\,\mathrm{m\,s^{-1}}$, and $1480\,\mathrm{m\,s^{-1}}$ of distilled water.

Figure 5 shows 5-MHz brightness-mode scans of a phantom receptacle well with a 28-mm bore diameter and their respective axial profiles. Although nucleation activity was visible in the circular areas in frames (a–d), the speed of sound in the ink was not observed to change, nor the attenuation coefficient, which remained steady at $0.15\pm0.01\,\mathrm{dB\,cm^{-1}\,MHz^{-1}}$ at this frequency. As the sonicating frequency was approximately one third of the resonance frequency, only stable cavitation and dissolution were to be expected in this acoustic regime.

The device amplification between the two interfaces was 6 dB for ink and 7 dB for saline (f). Contrary to the results at 13-MHz sonication, here the geometric and reflection contributions could not be neglected. The total signal amplification was 3 dB for ink and 8 dB for saline. This amplification is clearly visible at distances greater than the distal interface. The axial cross section from the well filled with phantom material shows a steady decline, supporting the slight difference in attenuation with respect to the device compensation.

In the tubes and capillaries, the ink had been diluted to 25% to make flow into the receptacle possible. Scattering from ink particles inside these receptacles was not observed. Therefore, the influence of dilution on the transient nature and the quantity of acoustic scatterers could not be established. Figure 6 shows brightness-mode scans of capillaries with a 0.20-mm bore diameter and their respective axial profiles.

As the wavelength of the 13-MHz ultrasound in water, approximately 0.12 mm, is less than the diameter of the capillary, two capillary walls should be visible if the acoustic impedance difference is sufficiently high. The axial backscattering in the ink-filled capillary had peak 8-bit gray levels of 95 and 114, respectively. The acoustic impedance difference was high enough to make both capillary walls visible. The peak-to-peak distance of 0.28 mm approximated the capillary width.

The backscattering of the water-filled capillary had a peak gray level of 68. Here, no separate walls were visible. This cannot be attributed to the capillary being outside the elevation plane, as the 0.22-mm outer capillary diameter is substantially less than the transducer elevation. The contribution to the acoustic response can be fully attributed to the cellulose material, as the medium inside the capillary was the same as outside. The backscattering of the air-filled capillary had one peak level of 233. Here, separate walls were not visible either. The long axial scattering zone of 0.99 mm (gray level threshold of 20) is explained from the linear oscillating dynamics of the air trapped in the capillary, which responded to the incident sound field. The resonance frequency of the air-filled capillary was less than 50 kHz, too far from the incident sound field

frequency to cause any other dynamic effect [31].

These results show that there was a clear acoustic impedance difference between water and black ink. Thus, the black ink acted as a reflector, although it was in 25% dilution. This outcome limits absolute quantification from distal scatterers, as the transmitted ultrasound pulse may have changed when passing through an inked region.

IV. Conclusions

In this study, brightness-mode sonography was performed on ink-filled receptacles, using pulsed ultrasound with center frequencies of 13 MHz and 5 MHz.

The attenuation coefficient of ink was measured to be $0.15\pm0.01\,\mathrm{dB\,cm^{-1}\,MHz^{-1}}$, of saline $0.02\pm0.02\,\mathrm{dB\,cm^{-1}\,MHz^{-1}}$, and of distilled water $0.00\pm0.01\,\mathrm{dB\,cm^{-1}\,MHz^{-1}}$. The speed of sound of tattoo ink in steady-state was measured to be $1639\,\mathrm{m\,s^{-1}}$, of saline $1568\,\mathrm{m\,s^{-1}}$, and of distilled water $1480\,\mathrm{m\,s^{-1}}$.

Transient scattering from the ink was observed. Backscattering from distal phantom materials was amplified by the presence of carbon black.

The speed of sound in ink was observed to drop to transiently to $1621\,\mathrm{m\,s^{-1}}$ for less than ten minutes during 13-MHz sonication, but not during 5-MHz sonication. The drop in speed at 13-MHz sonication may be attributed to strong, yet transient, cavitation activity, as the resonance frequency of the largest hydrophobic carbon black nanoparticles is 15 MHz.

This finding is useful for the potential deposition of acoustic energy into tattoos with the purpose of modifying them.

Acknowledgments

The sonography equipment was kindly supplied by High Tech Medical, Randburg, South Africa. Laser scanning confocal microscopy was performed at the Life Sciences Imaging Facility of the University of the Witwatersrand, Johannesburg. This work has been based on research supported in part by the National Research Foundation of South Africa, Grant Number 127102.

References

[1] M.L. Armstrong: “Career-oriented women with tattoos”, *Journal of Nursing Scholarship*, Vol. 23, No. 4, pp. 215–220, 1991.

[2] M.T. French, K. Mortensen and A.R. Timming: “Are tattoos associated with employment and wage discrimination? Analyzing the relationships between body art and labor market outcomes”, *Human Relations*, Vol. 72, No. 5, pp. 962–987, 2019.

[3] G.E. Long and L.S. Rickman: “Infectious complications of tattoos”, *Clinical Infectious Diseases*, Vol. 18, No. 4, pp. 610–619, 1994.

[4] J. Kazandjieva and N. Tsankov: “Tattoos: dermatological complications”, *Clinics in Dermatology*, Vol. 25, No. 4, pp. 375–382, 2007.

[5] N. Kluger and V. Koljonen: “Tattoos, inks, and cancer”, *Lancet Oncology*, Vol. 13, No. 4, pp. e161–e168, 2012.

[6] K. Hutton Carlsen and J. Serup: “Patients with tattoo reactions have reduced quality of life and suffer from itch: Dermatology Life Quality Index and Itch Severity Score measurements”, *Skin Research & Technology*, Vol. 21, No. 1, pp. 101–107, 2015.

[7] G.G. Grumet: “Psychodynamic implications of tattoos”, *American Journal of Orthopsychiatry*, Vol. 53, No. 3, pp. 482–492, 1983.

[8] S.T. Carroll, R.H. Riffenburgh, T.A. Roberts and E.B. Myhre: “Tattoos and body piercings as indicators of adolescent risk-taking behaviors”, *Pediatrics*, Vol. 109, No. 6, pp. 1021–1027, 2002.

[9] K. Hutton Carlsen, J. Tolstrup and J. Serup: “High-frequency ultrasound imaging of tattoo reactions with histopathology as a comparative method: introduction of preoperative ultrasound diagnostics as a guide to therapeutic intervention”, *Skin Research & Technology*, Vol. 20, No. 3, pp. 257–264, 2014.

[10] J. Serup: “Diagnostic tools for doctor’s evaluation of tattoo complications”, *Current Problems in Dermatology*, Vol. 52, pp. 42–57, 2017.

[11] M. Kuperman-Beade, V.J. Levine and R. Ashinoff: “Laser removal of tattoos”, *American Journal of Clinical Dermatology*, Vol. 2, No. 1, pp. 21–25, 2001.

[12] D. Hazlewood and X. Yang: “Enhanced laser surface ablation with an integrated photoacoustic imaging and high intensity focused ultrasound system”, *Lasers in Surgery and Medicine*, Vol. 51, No. 7, pp. 616–624, 2019.

[13] J. Serup, T. Bove, T. Zawada, A. Jessen and M. Poli: “High-frequency (20 MHz) high-intensity focused ultrasound: new ablative method for color-independent tattoo removal in 1-3 sessions. An open-label exploratory study”, *Skin Research & Technology*, DOI: 10.1111/srt.12885, 2020.

[14] Y. Eklund and A. Troilius Rubin: “Laser tattoo removal, precautions, and unwanted effects”, *Current Problems in Dermatology*, Vol. 48, pp. 88–96, 2015.

[15] N.R. Jacobsen and P.A. Clausen: “Carbon black nanoparticles and other problematic constituents of black ink and their potential to harm tattooed humans”, *Current Problems in Dermatology*, Vol. 48, pp. 170–175, 2015.

[16] T. Høgsberg, K. Hutton Carlsen and J. Serup: “High prevalence of minor symptoms in tattoos among a young population tattooed with carbon black and organic pigments”, *Journal of the European Academy of Dermatology and Venereology*, Vol. 27, No. 7, pp. 846–852, 2013.

[17] T. Høgsberg, K. Loeschner, D. Löf and J. Serup: “Tattoo inks in general usage contain nanoparticles”, *British Journal of Dermatology*, Vol. 165, No. 6, pp. 1210–1218, 2011.

[18] A. Humphries, T.S. Lister, P.A. Wright and M.P. Hughes: “Determination of the thermal and physical properties of black tattoo ink using compound analysis”, *Lasers in Medical Science*, Vol. 28, No. 4, pp. 1107–1112, 2013.

[19] M. Postema, R. Matsumoto, R. Shimizu, A.T. Poortinga and N. Kudo: “High-speed footage shows transient ultrasonic nucleation of different hydrophobic particles in suspension”, *Japanese Journal of Applied Physics*, Vol. 59, No. SKKD07, 2020.

[20] M. Postema, S. Phadke, A. Novel, R. Uzbekov, C. Nyamupangedengu, M. Anouti and A. Bouakaz: “Ultrasonic identification technique in recycling of lithium ion batteries”, *Proceedings: IEEE AFRICON*, No. 9133954, 2019.

[21] J.C. Bamber: “Ultrasonic attenuation in fresh human tissues”, *Ultrasonics*, Vol. 19, No. 4, pp. 187–188, 1981.

[22] F.A. Duck: *Physical Properties of Tissue: A Comprehensive Reference Book*, Academic Press, London, 1990.

[23] W. Secomski, A. Nowicki and P. Tortoli: “Estimation of hematocrit by means of attenuation measurement of ultrasonic wave in human blood”, *Proceedings: IEEE Ultrasonics Symposium*, Vol. 2, pp. 1277–1280, 2001.

[24] M.M. Calor-Filho and J.C. Machado: “Measurement of the ultrasonic attenuation coefficient of human blood plasma during clotting in the frequency range of 8 to 22 MHz”, *Ultrasound in Medicine & Biology*, Vol. 32, No. 7, pp. 1055–1064, 2006.

[25] B. Patterson and D.L. Miller: “Experimental measurements of ultrasound attenuation in human chest wall and assessment of the mechanical index for lung ultrasound”, *Ultrasound in Medicine & Biology*, Vol. 46, No. 6, pp. 1442–1454, 2020.

[26] T. Yoshida and T. Kondo: “Measurement on ultrasonic attenuation coefficient of tissue mimicking materials”, *Proceedings: Symposium on Ultrasonic Electronics*, Vol. 30, pp. 23–24, 2009.

[27] A.I. Farrer, H. Odéen, J. de Bever, B. Coats, D.L. Parker, A. Payne and D.A. Christensen: “Characterization and evaluation of tissue-mimicking gelatin phantoms for use with MRgFUS”, *Journal of Therapeutic Ultrasound*, Vol. 3, No. 9, 2015.

[28] C.-T. Chen, L.-S. Chen and F.J. Millero: “Speed of sound in NaCl, $MgCl_2$, Na_2SO_4, and $MgSO_4$ aqueous solutions as a function of concentration, temperature, and pressure”, *Journal of the Acoustical Society of America*, Vol. 63, No. 6, pp. 1795–1800, 1978.

[29] S.J. Kleis and L.A. Sanchez: “Dependence of speed of sound on salinity and temperature in concentrated NaCl solutions”, *Solar Energy*, Vol. 45, No. 4, pp. 201–206, 1990.

[30] E. Franceschini, F.T.H. Yu, F. Destrempes and G. Cloutier: “Ultrasound characterization of red blood cell aggregation with intervening attenu-

ating tissue-mimicking phantoms", *Journal of the Acoustic Society of America*, Vol. 127, No. 2, pp. 1104–1115, 2010.

[31] M. Postema: *Fundamentals of Medical Ultrasonics*, Taylor & Francis, London, 2011.

[32] P. Attard: "Nanobubbles and hydrophobic attraction", *Advances in Colloid and Interface Science*, Vol. 104, No. 1–3, pp. 75–91, 2003.

[33] T.G. Leighton: *The Acoustic Bubble*, Academic Press, London, 1994.

[34] M. Postema, R. Matsumoto, R. Shimizu, A.T. Poortinga and N. Kudo: "Ultrasound homogenises suspensions of hydrophobic particles", *Proceedings: Symposium on UltraSonic Electronics*, Vol. 40, No. 2E2-4, 2019.

[35] N. Kudo, R. Uzbekov, R. Matsumoto, R. Shimizu, C.S. Carlson, N. Anderton, A. Deroubaix, C. Penny, A.T. Poortinga, D.M. Rubin, A. Bouakaz and M. Postema: "Asymmetric oscillations of endoskeletal antibubbles", *Japanese Journal of Applied Physics*, Vol. 59, No. SKKE02, 2020.

[36] K. Johansen and M. Postema: "Lagrangian formalism for computing oscillations of spherically symmetric encapsulated acoustic antibubbles", *Hydroacoustics*, Vol. 19, pp. 197–208, 2016.

[37] J. Teng: *Ultrasound: An Alternative Solution to Removing Tattoos*, Dissertation, Massachusetts Institute of Technology, 2005.

[38] C.A. Grant, P.C. Twigg, R. Baker and D.J. Tobin: "Tattoo ink nanoparticles in skin tissue and fibroblasts", *Beilstein Journal of Nanotechnology*, Vol. 6, No. 1, pp. 1183–1191, 2015.

[39] A. Deroubaix, B. Moahla and C. Penny: "Monitoring of intracellular localization of Hepatitis B virus P22 protein using Laser Scanning Confocal Microscopy and Airyscan", *Microscopy Research & Technique*, Vol. 83, No. 5, pp. 499–506, 2020.

[40] M. Nathan: *Ultrasonic Blood Fractionation*, Dissertation, University of the Witwatersrand, Johannesburg, 2020.

[41] C. Smalberger: *Ultrasound-Assisted Cell Eradication*, Dissertation, University of the Witwatersrand, Johannesburg, 2020.

[42] G. ter Haar: "Ultrasonic imaging: safety considerations", *Interface Focus*, Vol. 1, No. 4, pp. 686–697, 2011.

[43] R.O. Bude and R.S. Adler: "An easily made, low-cost, tissue-like ultrasound phantom material", *Journal of Clinical Ultrasound*, Vol. 23, No. 4, pp. 271–273, 1995.

[44] K. Attenborough and M. Postema: *A pocket-sized introduction to acoustics*, University of Hull, Kingston upon Hull, 2008.

Craig S. Carlson (SIEEE'08–M'12–MSAIEE'14) received the B.Sc. degree in Electrical Engineering from the University of the Witwatersrand, Johannesburg, South Africa, in 2009, the M.Sc. degree in Engineering from the University of the Witwatersrand, Johannesburg, in 2012, and the M.B.A. degree from the University of Pretoria, South Africa, in 2018. He is an Associate Lecturer in Biomedical Engineering at the University of the Witwatersrand, Johannesburg. His research interests include other-than-diagnostic uses of medical ultrasound, sharp sonic cutting, tattoo modification, and tattoo removal.

Aurélie Deroubaix received the M.Sc. degree in Life and Health Sciences, Microbiology and Immunology from the University of Bordeaux, France, in 2008, and the Ph.D. degree in Microbiology and Virology from the University of Bordeaux in 2011. She did her post-doctoral studies at the University of the Witwatersrand, Johannesburg, South Africa from 2012 to 2015. She was appointed Manager of the Microscopy Unit (Life Sciences Imaging Facility) at the Medical School of the University of the Witwatersrand, Johannesburg, as Senior Microscopy Technician in 2015 and Senior Lecturer in 2016. She was also appointed Associate Researcher in the Hepatitis Virus Diversity Research Unit in 2016. She works on Hepatitis B virus-associated hepatocellular carcinoma.

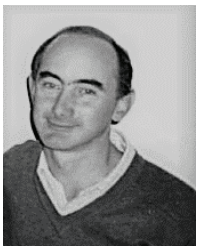

Clement Penny received the Ph.D. in Developmental Biology from the University of the Witwatersrand, Johannesburg, South Africa, in 2004. He is presently the Chair of the Human Research Ethics Committee (Medical), and Senior Research Scientist, with a joint appointment with the JHB Oncology Research Division at the Wits Health Consortium and the University of the Witwatersrand Medical Oncology Division; and is a member of the Wits-MRC Common Epithelial Cancer Research Centre and the Wits Advanced Drug Delivery Platform. His research interests include understanding the role of cancer stem cells in colorectal cancer in association with the poorly understood early-onset thereof in young South Africans.

Michiel Postema (AIEEE'01–S'02–M'05–SM'08) received the M.Sc. degree in Geophysics from Utrecht University, The Netherlands, in 1996, the Ph.D. degree in Physics from the University of Twente, The Netherlands, in 2004, and the Habilitation à Diriger des Recherches (D.Sc.) degree in Life and Health Sciences from the University of Tours, France, in 2018. He was appointed Professor of Experimental Acoustics at the Universtiy of Bergen, Norway, in 2010, Professor of Ultrasonics at the Polish Academy of Sciences in 2016, Distinguished Professor of Biomedical Engineering at the University of the Witwatersrand, Johannesburg, South Africa, in 2018, and Professor of Medical Physics at Tampere University, Finland, in 2020. He works with medical microparticles under sonication and in high-speed photography.

CONTENTS PAGE